Annual Cycle of Equatorial East–West Circulation over the Indian and Pacific Oceans

TAKIO MURAKAMI AND BIN WANG

Department of Meteorology, School of Ocean and Earth Science and Technology, University of Hawaii, Honolulu, Hawaii

(Manuscript received 11 March 1991, in final form 27 August 1992)

ABSTRACT

Along the equator, annual mean 200-mb zonal wind is approximately in phase with annual mean outgoing longwave radiation (OLR); namely, easterlies are strongest above the convective center over the maritime continent, while westerlies reach their maximum just above the dry zone over the equatorial Pacific. This is much different from what is anticipated by theories that predict that the phase of the upper-tropospheric zonal wind is in quadrature with that of the prescribed heating. The present study provides evidence that the midlatitude–equatorial coupling is primarily responsible for the maintenance of the annual mean total 200-mb zonal winds along the equator, whereas convection contributes a great deal to the annual mean upper-level equatorial divergent winds. Annual cycles occurring over the extratropics act as a transient eddy forcing of the equatorial annual mean 200-mb zonal wind through three-dimensional convergence of localized Eliassen–Palm (E–P) fluxes. They are acting to accelerate the 200-mb annual mean westerlies (easterlies) over the equatorial eastern Pacific (Indian Ocean) where E–P fluxes are horizontally divergent (convergent). The baroclinic contribution, acting through the meridional heat flux due to annual cycles, appears to be minimal.

The annual cycles differ remarkably between the equatorial Indian and eastern Pacific oceans. The annual cycle in the equatorial Indian Ocean is characterized by 1) the eastward phase propagation of monthly mean anomaly zonal winds with an inverse relationship between the surface and 200 mb (i.e., baroclinic structure in the vertical), and 2) the highest SST occurring about three (four) months prior to the strongest surface westerlies (minimum OLR). The annual cycle in the equatorial eastern Pacific exhibits coherent westward propagation of monthly mean anomaly SST and surface zonal winds, indicating the importance of planetary boundary-layer processes. On the other hand, the annual cycle of 200-mb equatorial zonal winds (the upper-level east–west circulation) is largely of standing wave character, while the annual cycle of OLR is of propagating wave character, implying that the equatorial convection contributes little to the annual cycle of the upper-level east–west equatorial circulation. It is shown that the annual cycle in the upper-level zonal winds over the equatorial eastern Pacific is largely controlled by a pronounced annual cycle of the 200-mb zonal wind occurring in the extratropics of each hemisphere.

1. Introduction

The annual cycles of the tropical atmosphere and ocean have been comprehensively described in a number of atlases of monthly means derived from ship and island observations (Taylor 1973; Wyrtki and Meyers 1975; Hastenrath and Lamb 1978; Weare et al. 1980; Sadler et al. 1987). Based upon these useful databases, many subtle and significant signals have been delineated. The annual cycle in surface winds is primarily dominated by meridional migration of the trade-wind belts of both hemispheres (Wyrtki and Meyers 1976). The annual cycles in sea level pressure and rainfall have been documented in terms of the amplitude and phase of the annual and semiannual harmonics (Hsu and Wallace 1976; Dorman and Bourke 1979; Wang 1992a). An extensive investigation of annual cycles in sea level pressure, surface winds, sea surface temperature (SST), and precipitation over the Pacific was carried out by Horel (1982). He showed that 1) annual cycles in horizontal pressure gradient are kinematically consistent with the corresponding cycles in wind speed over the tropics, and 2) the annual cycles in rainfall and surface convergence have some common features, particularly in the equatorial regions dominated by convection.

It has been recognized in recent years that interannual variability, especially variability associated with the El Niño–Southern Oscillation (ENSO), is closely related to the annual variability. For instance, the annual cycle seems to play an active role in modifying El Niño (Ramage and Hori 1981; Rasmusson and Carpenter 1982); a strong and weak annual cycle in the tropical Indian and western Pacific oceans tends to correspond to, respectively, El Niño and La Niña (Meehl 1987); the biennial mode of ENSO variability is tightly phase locked with the interannual variation of the annual cycle (Rasmusson et al. 1990). Furthermore, the annual cycle involves, to some extent, air–sea interactions possibly similar to those that determine the Southern Oscillation (Philander 1990). The sys-

Corresponding author address: Prof. Bin Wang, Department of Meteorology, University of Hawaii at Manoa, School of Ocean and Earth Sci. and Tech., 2525 Correa Road, Honolulu, HI 96822.

tematic phase change in the annual cycle of SST in the eastern Pacific is evidently correlated with annual cycles in surface winds, suggesting air–sea interactions occurring on an annual time scale (Horel 1982). Another example is the coherence between the annual march of the intertropical convergence zone (ITCZ) and annual changes in surface winds and SST in the cold-tongue region of the equatorial eastern Pacific (Wallace et al. 1989). Mitchell (1990) noticed an interaction between continental and oceanic convection in the America–Africa sector and spring–fall asymmetry in equatorial convection over this region. The close connection between annual and ENSO variabilities makes it necessary to examine the annual variability of the tropical atmosphere and ocean in order to fully understand ENSO variability.

This study investigates the annual cycle of the atmospheric circulation and SST over the global tropics: in particular, the equatorial Pacific and Indian oceans, which are the core regions of ENSO variability. In this equatorial waveguide, the ocean mixed layer tends to respond to changes in zonal wind stress most sensitively. The annual cycle of the zonally oriented Walker circulation is a major focus of the present study. Bjerknes (1969) defined the Walker circulation as a thermal circulation driven by the gradient of sea surface temperature along the equator. The updraft portion was inferred from the profile of surface pressure. This is subject to some ambiguity. In the present study, the updraft center was determined from outgoing longwave radiation (OLR) data averaged over an equatorial belt from 5°S to 5°N. The updraft center was also identified from the upper-level divergent wind field, which is generally in good agreement with OLR. Although the divergent winds well reflect a thermal circulation, the investigation into air–sea interaction requires the total surface winds, rather than the divergent part of winds alone. For this reason, the equatorial east–west (E–W) circulation, as defined in this study, refers to the longitudinal distribution of total zonal winds. Its annual cycle is described in terms of month-to-month variations of anomaly zonal winds. The annual cycles of SST and atmospheric variables away from the equator can largely be explained by the annual cycle in solar heating and associated thermal and dynamical processes. However, the annual variation in the equatorial region is much more complex due to the involvement of the monsoons, trade winds, and midlatitude influences and the complex air–sea–land interactions.

We first document the annual mean fields in section 3, following a brief description of the data and methodology in section 2. In section 4 the physical processes that maintain the annual mean equatorial E–W circulation are examined, with particular attention paid to the July and January mean wind fields over the global tropics. Section 5 describes annual cycles of the E–W circulation over the equatorial Indian and Pacific oceans. The last section summarizes our primary results.

2. Data

The datasets used in the present research include the climatological monthly mean fields of SST, sea level pressure (p_s), and surface zonal (u_s) and meridional (v_s) winds derived from the Comprehensive Ocean–Atmosphere Data Set (COADS) for the period 1900–1979 by Sadler et al. (1987), the climatological monthly mean OLR derived from NOAA satellite observations for a 10-year period 1975–1977 and 1979–1985, and the climatological monthly mean 200-mb zonal (u_{200}) and meridional (v_{200}) winds derived from the ECMWF (European Centre for Medium-Range Weather Forecasts) gridded global analysis for the period 1980–1987.

OLR data are used to infer the amount of deep convection and rainfall in the tropics. This is based upon a reliable and good negative correlation between monthly rainfall and OLR (e.g., Motell and Weare 1987). In view of the scarcity of rainfall data in the tropics, OLR data are valuable for deducing deep convection, rainfall, heat sources, and vertical motion. The inferences, however, must be regarded as an approximation to these quantities, but with firm qualitative confidence.

During the eight-year period 1980–1987, the analysis and initialization scheme used at ECMWF changed considerably. Trenberth and Olsen (1988) carefully evaluated ECMWF analysis and pointed out its frailties and weaknesses. In particular, the divergent part of winds appears to be quite small; however, the monthly mean velocity potential field computed from ECMWF wind data turns out to be well correlated with the monthly mean OLR pattern. Encouraged by this agreement, we use in the present study the ECMWF climatological monthly mean wind analyses as the basic dataset for the investigation into annual cycles over the global tropics from 40°N to 40°S.

For each variable, the climatological monthly mean fields are decomposed into annual means, annual and semiannual harmonics, and a residual, using Fourier analysis in the time domain. The annual variation of a variable is referred to as "month-to-month changes" in its 12 monthly mean anomalies with reference to the corresponding annual mean, and is denoted by an asterisk ( )*.

3. Annual mean perturbation

This section investigates the annual mean climatology. The notation $\langle\ \rangle$ is introduced to signify the annual mean.

a. Annual mean perturbation along the equator

Figure 1 is prepared to investigate the phase relationship among the annual mean $\langle u_s \rangle$ and $\langle u_{200} \rangle$ (a), $\langle \mathrm{SST} \rangle$ and $\langle \mathrm{OLR} \rangle$ (b), and $\langle p_s \rangle$, $\langle v_s \rangle$, and $\langle v_{200} \rangle$ (c) perturbations along the equator. An approximate out-of-phase relationship exists between $\langle u_s \rangle$ and

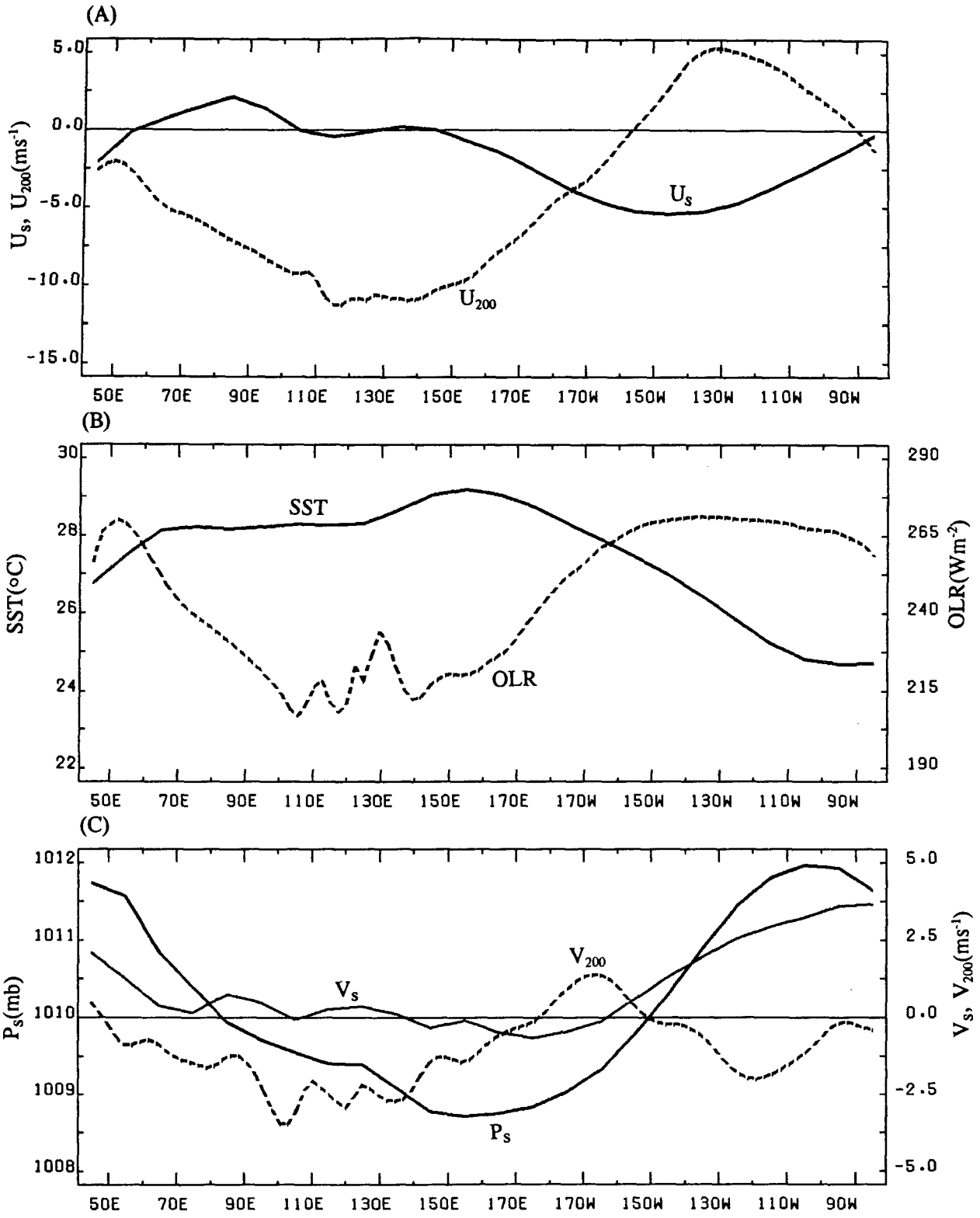

FIG. 1. Annual mean perturbations along the equator averaged between 5°N and 5°S: (a) 200-mb and surface zonal winds, (b) SST and OLR, and (c) 200-mb and surface meridional winds, and surface pressure.

$\langle u_{200} \rangle$, indicating that the annual mean zonal wind perturbation along the equator is of baroclinic structure in the vertical. The upper-level branch of the equatorial E–W circulation is defined by $\langle u_{200} \rangle$ westerlies (easterlies) to the east (west) of about 160°W. The low-level branch of the E–W circulation is signified by surface easterlies (westerlies) over the eastern and central Pacific (the western Pacific and eastern Indian Ocean). In Fig. 1b, one notes an approximate association of low $\langle$SST$\rangle$ with high $\langle$OLR$\rangle$, and high $\langle$SST$\rangle$ with low $\langle$OLR$\rangle$. Thus, it appears that $\langle$SST$\rangle$ is responsible, at least partially, for the enhancement of convection over the maritime continent (100°–150°E), which corresponds to an updraft portion of the annual mean E–W circulation. A comparison between Figs. 1a and 1c displays a $\langle u_s \rangle$ wind perturbation in quadrature with a $\langle p_s \rangle$ perturbation. Roughly speaking, $\langle u_s \rangle$ is westerly (easterly) in regions of negative (positive) zonal $\langle p_s \rangle$ gradient along the equator. Figure 1c further illustrates that everywhere along the equator, $\langle v_s \rangle$ is negatively correlated with $\langle v_{200} \rangle$. For example, the annual mean local Hadley cell along 120°W is associated with the cross-equatorial surface southerlies as its low-level branch, while the cross-equatorial 200-mb northerlies representing its upper-level branch.

The most important implication in Fig. 1 is that $\langle$OLR$\rangle$ is nearly in phase with $\langle u_{200} \rangle$, while approximately out of phase with $\langle u_s \rangle$. This indicates that the negative $\langle$OLR$\rangle$ anomaly is in quadrature with the east–west $\langle u_{200} \rangle$ zonal divergence and/or $\langle u_s \rangle$ zonal convergence anomaly. The downdraft leg of the E–W circulation appears to be located over the eastern Pacific around 130°–140°W, where $\langle$OLR$\rangle$ is a maximum (persistent dry weather). Yet, neither east–west $\langle u_{200} \rangle$ convergence nor east–west $\langle u_s \rangle$ divergence is encountered in the immediate vicinity of the downdraft leg. The central equatorial Pacific around 170°E–160°W is characterized by a major east–west $\langle u_s \rangle$ convergence, capped by a maximum east–west $\langle u_{200} \rangle$ divergence. This region cannot, however, be identified as an updraft portion of the equatorial E–W circulation, since convection is inactive over the equatorial central Pacific. On the other hand, the convectively active maritime continent (100°–150°E) is a region of near-zero east–west convergence (divergence) in $\langle u_s \rangle$ ($\langle u_{200} \rangle$). Hence, both $\langle u_s \rangle$ and $\langle u_{200} \rangle$ zonal wind perturbations contribute little to the annual mean convective activity over the maritime continent. Farther to the west over the central Indian Ocean (80°–100°E), $\langle u_s \rangle$ westerlies and $\langle u_{200} \rangle$ easterlies are both converging, which is not congruent with a substantially low $\langle$OLR$\rangle$ of about 230 W m^{-2}. In summary, everywhere along the equator, $\langle$OLR$\rangle$ is essentially not correlated with an east–west convergence anomaly in the surface and 200-mb zonal wind perturbations.

The local Hadley circulation, which is associated with both the surface and 200-mb meridional winds, appears to play a crucial role in determining a net local convergence along the equator. At the surface (200 mb) over the equatorial central Pacific, an east–west $\langle u_s \rangle$ convergence ($\langle u_{200} \rangle$ divergence) is overcompensated for by a prominent north–south $\langle v_s \rangle$ divergence ($\langle v_{200} \rangle$ convergence), which is implied by the downdraft and persistent dry weather (high $\langle$OLR$\rangle$) there. Over the maritime continent between 100° and 150°E, the annual mean convective activity must be supported by strong north–south $\langle v_s \rangle$ convergence and north–south $\langle v_{200} \rangle$ divergence, because the contribution to total vergence due to $\langle u_s \rangle$ and $\langle u_{200} \rangle$ is minimal, as stated earlier. Similarly, over the equatorial Indian Ocean, the Hadley-type north–south vertical overturning ($\langle v_s \rangle$ and $\langle v_{200} \rangle$) contributes most to the net local convergence. These points will further be elaborated on later.

The foregoing property of the annual mean E–W circulation along the equator is much different from what is anticipated by theories on the atmospheric response to a prescribed equatorial heat source (Gill 1980; Lim and Chang 1983; Lau and Lim 1984). All theories predict an east–west upper-level divergence and/or low-level convergence anomaly in phase with the prescribed heating. Accordingly, the model-produced upper-level westerlies (low-level easterlies) are strongest at a quarter-wavelength eastward of the heating. Conversely, at a quarter-wavelength westward of the heating are the strongest upper-level easterlies (low-level westerlies). These model-predicted zonal winds are at odds with the observed annual mean $\langle u_{200} \rangle$ and $\langle u_s \rangle$ zonal winds in Fig. 1a. The observed $\langle u_s \rangle$ westerlies are strongest (2.1 m s^{-1}) at the central Indian Ocean near 80°E, that is, at a halfway point between the downdraft leg (cooling) off the east coast of Africa and the updraft leg (heating) over the maritime continent. This is in qualitative agreement with Gill's solution. The observed $\langle u_{200} \rangle$ easterlies are not strongest near 80°E, however, but maximum around 100°–150°E, that is, just above the updraft leg (heating) over the maritime continent. Similarly, right above the downdraft leg (cooling) over the eastern equatorial Pacific around 130°W are the strongest $\langle u_{200} \rangle$ westerlies overlaying the most intense $\langle u_s \rangle$ easterlies. As such, a large difference exists between the observed and model-produced zonal wind perturbations along the equator. Such disagreement leads us to question whether or not the annual mean heating as determined by $\langle$OLR$\rangle$ along the equator is really responsible for the enhancement of equatorial $\langle u_s \rangle$ and $\langle u_{200} \rangle$ perturbations. Other questions that need to be addressed include: What influence does the annual cycle have in maintaining the annual mean zonal wind perturbations? To what extent do the extratropics of both hemispheres exert some measure of control upon the equatorial zonal wind perturbations? In an effort to answer these questions, the next subsection provides additional information on the global aspects of annual mean perturbations from 40°N to 40°S.

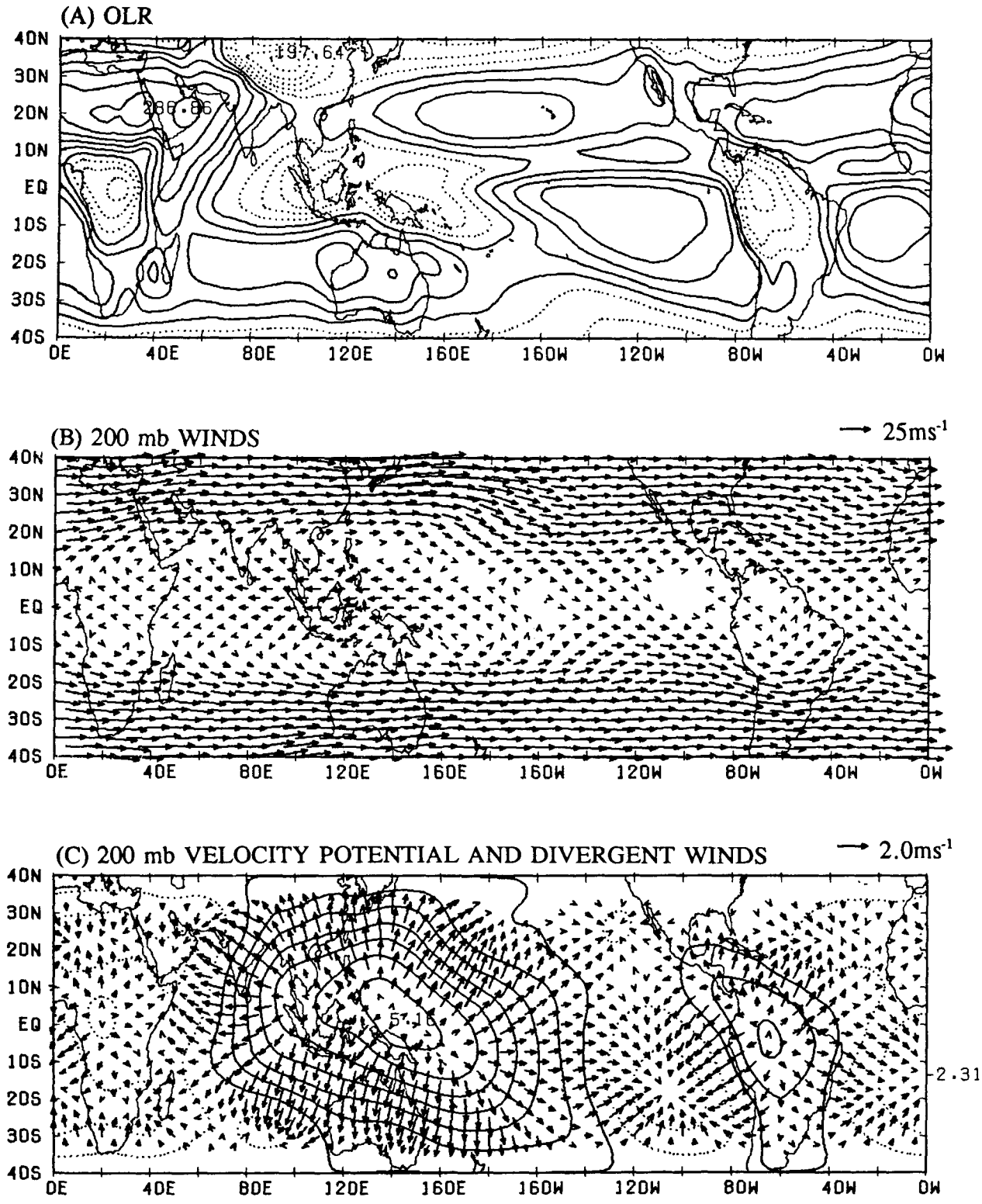

FIG. 2. Annual mean patterns of (a) OLR (interval 8 W m^{-2}, dashed lines less than 232 W m^{-2}), (b) 200-mb winds, and (c) velocity potential (interval 0.8×10^6 m^2 s^{-1}, dashed lines less than zero) and divergent winds.

b. Annual mean OLR and 200-mb circulation over the global tropics

In Fig. 2a, the annual mean $\langle \text{OLR} \rangle$ is less than 224 W m^{-2} over equatorial Africa (10°–30°E) and equatorial South America (60°–80°W). These are two equatorial continents of active convection throughout the year. Accordingly, the effect of continentality appears to be as important as, or even more important than, the SST effect in enhancing active convection along the equator. The $\langle \text{OLR} \rangle$ is also less than 224 W m^{-2} over Indonesia between about 90°E and 160°E. Although Indonesia is in the middle of the world's warmest SST pool, it may act, in some ways, like a very moist continent (commonly termed a maritime continent). Near these convectively active equatorial landmasses, $\langle \text{OLR} \rangle$ is approximately symmetric about the equator. Over the eastern sectors of the Pacific and Atlantic oceans, however, $\langle \text{OLR} \rangle$ is asymmetric with reference to the equator with the minimum $\langle \text{OLR} \rangle$ around 10°N (the eastern Pacific) or 5°N (the eastern Atlantic). In general, these latitudes are characterized by the highest $\langle \text{SST} \rangle$, implying the coincidence of the thermal equator with the most active convective zone.

Gill (1980) showed that the atmospheric response to a symmetric heat source is trapped in an equatorial duct, which is determined by the equatorial Rossby deformation radius and extends about 15 degrees of latitude away from the equator. At the upper troposphere, west of the prescribed heating is a Rossby wave response with upper-level easterlies sandwiched between two identical anticyclonic centers straddling the equator. East of the forcing is a Kelvin wave response with the strongest upper-level westerlies along the equator. The Kelvin wave response has an appreciable secondary circulation in the equatorial plane and is often referred to as the divergent part of the E–W circulation (Krishnamurti 1971).

A glance at Fig. 2b indicates that the observed 200-mb equatorial westerlies are not trapped in the equatorial latitudes, but occur as a part of a westerly duct that stretches across the eastern North and South Pacific and, thus, bridges the two hemispheres. This westerly duct is most pronounced along about 120°–150°W due to the equatorward penetration of midlatitude westerlies in and around the upper-tropospheric oceanic troughs over the eastern North and South Pacific. The meridional scale of the north–south extended westerly duct is on the order of 80° of latitude or even longer. Furthermore, the 200-mb equatorial westerlies near 130°W are strongest at some 80°–100° longitude away from the most active convective center near New Guinea. Perhaps there is no direct association between 200-mb westerlies over the eastern Pacific and equatorial convection over the maritime continent.

The meridional scale of the surface $\langle u_s \rangle$ trade winds is comparable to the corresponding scale of the 200-mb westerly duct. At 160°W, for instance, $\langle u_s \rangle$ is easterly at all latitudes between 30°N and 30°S with a maximum intensity (10 m s^{-1}) at 15°N (refer to the surface wind maps prepared by Sadler et al. 1987). Equatorward of that latitude, the $\langle u_s \rangle$ trades diminish considerably, amounting only to less than 5 m s^{-1} at the equator. In Fig. 1a, the equatorial E–W circulation was defined as an east–west vertical cell with the surface $\langle u_s \rangle$ trades capped by $\langle u_{200} \rangle$ westerlies along the equator over the central and eastern Pacific. The E–W circulation thus defined is not trapped in the equatorial latitudes; thus, it cannot be identified as a Kelvin response occurring to the east of heat sources along the equator. In fact, it is a part of the laterally extended east–west vertical cells (surface $\langle u_s \rangle$ easterlies capped by $\langle u_{200} \rangle$ westerlies aloft) with their maximum intensity not at the equator, but at subtropical latitudes in each hemisphere. This point should be kept in mind when examining the nature of the E–W circulation as defined along the equator.[1]

Over and west of the most active annual mean convection near the maritime continent are prominent equatorial 200-mb easterlies, which are sandwiched between the zonally oriented Northern Hemisphere ridge axis along about 15°N and the Southern Hemisphere counterpart around 10°S. Farther poleward, the Northern Hemisphere jet stream prevails near Japan and the Southern Hemisphere jet stream dominates Australia. Undoubtedly, the Japanese and Australian jet streams are enhanced by the annual mean local Hadley circulation, as pointed out by Sardeshmukh and Hoskins (1988). In Fig. 2c, the local Hadley circulation is defined by the annual mean divergent meridional wind $\langle v_{200} \rangle(\chi)$. Interestingly, $\langle v_{200} \rangle(\chi)$ is asymmetric about the equator, emanating from the upper-level outflow center over the maritime continent. In the Northern (Southern) Hemisphere, $\langle v_{200} \rangle(\chi)$ southerlies (northerlies) tend to accelerate the jet stream near Japan (Australia).

A comparison between Figs. 2a and 2c reveals an approximate agreement between convective centers (low $\langle \text{OLR} \rangle$) and divergent outflow centers (high $\langle \chi_{200} \rangle$) along the equator. The intensity of a local Hadley circulation can be measured by the magnitude of $\langle v_{200} \rangle(\chi)$. The local Hadley circulation appears to be most pronounced along about 130°E with the magnitude of $\langle v_{200} \rangle(\chi)$ exceeding 2 m s^{-1} near 25°N and 20°S, respectively. The intensity of $\langle v_{200} \rangle(\chi)$ is largely determined by the difference in diabatic heat sources between the equator and the midlatitudes. In addition, there is also a tendency for the equatorial $\langle u_{200} \rangle$ easterlies over the maritime continent to accelerate pole-

[1] As stated earlier, the E–W circulation is of approximate baroclinic character in the vertical. To facilitate the following discussion in the reminder of section 3, our attention will be focused on the structure of 200-mb zonal wind perturbations, that is, no further mention will be made of the surface zonal wind perturbations.

ward divergent $\langle v_{200} \rangle(\chi)$ flows due to the beta effect. On the other hand, the magnitude of zonal divergent winds [as signified by $\langle u_{200} \rangle(\chi)$] appears to be less pronounced, being only on the order of about 1 m s^{-1}. Over the western and central Pacific $\langle u_{200} \rangle(\chi)$ is westerly, emanating from the updraft center over the maritime continent and converging into the downdraft portion over the eastern Pacific. This westerly $\langle u_{200} \rangle(\chi)$ flow represents a divergent part of the equatorial E–W circulation over the equatorial Pacific. Note that a major part of the E–W circulation is nondivergent. The horizontal scale of the $\langle u_{200} \rangle(\chi)$ divergent cell, as measured by the longitudinal difference between the updraft and downdraft legs, is about 12 000 km, which is more than three times as large as the corresponding latitudinal scale of the local Hadley circulation. This may be one reason why the divergent E–W circulation along the equator is substantially weaker than the local Hadley circulation along 130°E. In general, the local Hadley circulation contributes most to the net local convergence field along the equator. These local Hadley circulations are thermally direct between about 80°E and 160°W (i.e., ascending warm equatorial air and descending cold midlatitude air), while they are thermally indirect between 140°W and 80°W (Fig. 2c). In general, the variability of $\langle u_{200} \rangle(\chi)$ along the equator is much smaller than the corresponding longitudinal variability of $\langle u_{200} \rangle$. For example, between 140°E and 130°W along the equator, $\langle u_{200} \rangle(\chi)$ changes from near zero to about 1.0 m s^{-1}, while $\langle u_{200} \rangle$ increases as much as 15 m s^{-1} from -10 m s^{-1} to $+5$ m s^{-1}.

In this subsection an attempt has been made to investigate the characteristic features of annual mean motions not only in the global tropics, but also in the extratropical latitudes of both hemispheres. Away from the equator, the motion fields exhibit a significant difference from one season to another. This seasonality and its possible contribution to the maintenance of annual mean perturbations over the tropics are investigated by comparing the July and January mean wind fields in the next section 4. Of course, we are aware that the annual cycle of any variable indicates the temporal asymmetry (or skewness) and, thus, the difference between the January and July mean variables is not an exact representation of the annual cycle. To save space, however, the monthly mean maps in other months (say, April and October) are not reproduced here.

4. July and January mean perturbations over the global tropics

a. July mean perturbations

In July when the northern summer is at its peak, both OLR and χ fields (Figs. 3a and 3c) exhibit distinct asymmetry with three major convective outflow centers about 10° to 15° of latitude north of the equator over North Africa, the Bay of Bengal–Philippines, and Central America, respectively. The July mean 200-mb winds are also largely asymmetric about the equator (Fig. 3b). The Northern Hemisphere is dominated by two prominent anticyclonic cells over Tibet and Mexico, with oceanic troughs over the Pacific and Atlantic oceans.

Poleward and equatorward divergent outflows from the Indochina–Philippines region represent the upper-level branch of the local Hadley circulation dominating the eastern hemisphere between about 90° and 150°E. One immediate effect of this local Hadley circulation is the enhancement of the wintertime jet stream near Australia, which is much stronger than the annual mean Australian jet (refer to Fig. 2b). In contrast, the summertime westerly jet near Japan becomes much less dominant than the annual mean jet.

Equatorward of the Tibetan anticyclone are prominent northeasterlies, eventually crossing the equator over the Indian Ocean (Fig. 3b). Thus, these northeasterlies carry easterly momentum into the Southern Hemisphere. In other words, there exists a northward flux of westerly momentum across the equator. Furthermore, the northeasterlies are generally subgeostrophic and, accordingly, cross the geopotential height contour from high to low. This results in an equatorward flux of wave energy that originates in regions of active monsoon rains over the Asiatic monsoon domain (refer to Murakami 1974a).

Of particular interest in Fig. 3 is that the Tibetan monsoon anticyclone is located some 30° to 50° longitude northwestward of the divergent center near the Philippines. The July mean rainfall over the southeastern Tibetan plateau amounts to only about 150 mm, which is less than one-half the rainfall over the summer monsoon region covering India, Indochina, the South China Sea, and the western North Pacific (Fig. 8.2 of Murakami 1987). This justifies the finding in Fig. 3c that the overall divergent center in July is located near the Philippines. Murakami (1974a,b) emphasized the importance of the beta effect as well as nonlinear effects (including the vorticity advection due to the divergent part of the winds) in maintaining the Tibetan anticyclone. Murakami's model was capable of reproducing the summer monsoon circulation with a distinct phase difference between the Tibetan anticyclone and the divergent outflow center. On the other hand, Sardeshmukh and Held (1984) made a detailed analysis of the vorticity balance of the summer mean flows obtained from numerical experiments. They showed that the vorticity balance is essentially inviscid, that is, has no need of a strong frictional damping of vorticity. These results are basically the same as those obtained in Murakami's (1974a,b) model experiment. Based on the three-year observed data from 1970 to 1972, Murakami (1978) confirmed that the divergent center is located near the Philippines, while the anticyclonic center is encountered over Tibet. Such phase difference was also emphasized in Young's

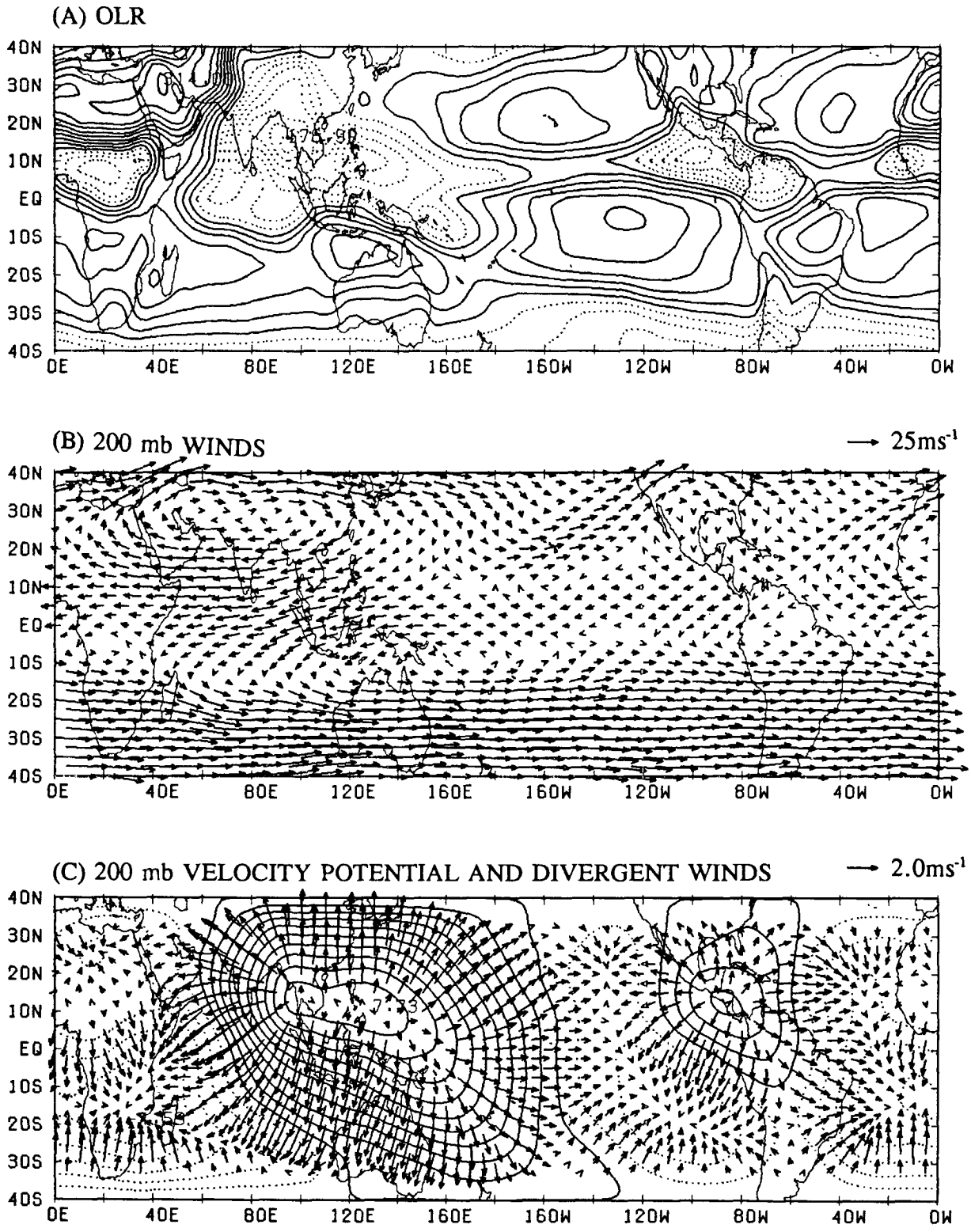

FIG. 3. As in Fig. 2 except for the July mean.

(1987) linear model with the beta effect included. He argued that when a heat source is prescribed away from the equator, the atmospheric response is confined to the heated region and neighboring western areas, in the form of Rossby and mixed Rossby–gravity waves. Conversely, no significant response occurs to the east;

that is, an eastern Kelvin wave response is weak. This agrees with the observed July mean wind fields shown in Fig. 3b, that is, the absence of the westerly over the equatorial Pacific.

b. *January mean perturbations*

The January mean OLR (Fig. 4a) and velocity potential (Fig. 4c) configurations are asymmetric about the equator. The Southern Hemisphere is dominated by three major divergent centers in the proximity of the equator, that is, about 5° to 10° of latitude south of the equator, around 30°E, 130°E, and 60°W, respectively. The Southern Hemisphere summer monsoon is most pronounced over the Indonesian seas and the western South Pacific. Between about 120°E and 150°E, the upper-level outflows from regions of heavy monsoon rains penetrate as far north as east China and Japan. This corresponds to the local Hadley circulation during southern summer. In association with the development of this local Hadley circulation, the wintertime jet stream near Japan intensifies considerably in contrast to the substantial weakening of the summertime jet stream over Australia.

There is a similar phase difference between the outflow centers and the anticyclonic centers. For example, the monsoon anticyclone over northwestern Australia is located some 20° longitude southwestward of the major outflow center at 5°S, 150°E. This Australian anticyclone in January is much less pronounced as compared with the Tibetan counterpart in July. The monsoonal easterlies prevailing equatorward of the Australian anticyclone are also much weaker.

Figure 4b reveals the dominance of strong equatorial westerlies over the eastern Pacific from about 160°W to 90°W with a maximum (15 m s^{-1}) at 130°W along the equator. The prominent westerlies over the equatorial eastern Pacific in January are largely associated with the enhanced westerly duct which, as pointed out by Murakami and Unninayar (1977), becomes most pronounced during northern winter. Webster and Holton (1982) were the first to note that a perturbation kinetic energy maximum was collocated with the westerly winds and that midlatitude waves could propagate through the westerly duct. The establishment of the strong westerly duct results from the development of the mid-Pacific troughs in both hemisphere subtropics. The development of the Northern Hemisphere trough is a downstream effect of the highly elevated and cooled Tibetan plateau, which enhances the western Pacific subtropical high and the mid–North Pacific trough. Thus, the Northern Hemisphere part of the westerly duct is largely controlled by the winter midlatitude circulation. On the other hand, the Southern Hemisphere counterpart of the westerly duct is not of midlatitude origin. This becomes evident when comparing July and January 200-mb winds (Figs. 3b and 4b). The equatorial westerlies over the southeastern Pacific occur in the southern summer (January), but not during the southern winter (July) when the midlatitude westerlies reach their maximum strength. In fact, the development of the Southern Hemisphere mid-Pacific trough is probably caused by the enhanced heating over the southern summer monsoon region from northern Australia to the South Pacific convergence zone (SPCZ). Therefore, it is reasonable to attribute the establishment of the strong westerly duct in January over the eastern tropical North and South Pacific to the combined effects of the tropical heating and midlatitude influences.

As the season advances to the northern summer, u_{200} over the equatorial eastern Pacific becomes slightly easterly (Fig. 3b). When averaged throughout the year, however, the annual mean u_{200} remains positive (westerly) and substantial (5 m s^{-1}) near 130°W at the equator. In short, the annual mean u_{200} equatorial westerlies are largely of wintertime extratropical origin. Much of the total annual mean zonal winds at the equator are due to processes that occur off the equator involved with the strong seasonal cycle.

Over the central Indian Ocean near 0°, 90°E, the u_{200} easterlies drastically decrease from 13.2 m s^{-1} in July (Fig. 3b) to 1.8 m s^{-1} in January (Fig. 4b). In July, the release of latent heat over the Asiatic summer monsoon domain induces strong atmospheric response, as indicated by prominent northeasterlies dominating the Indian Ocean (Fig. 3b). In comparison, the January mean convective activity over the south Indian Ocean is not as pronounced as that over Southeast Asia in July. Furthermore, the January mean convective zone is located very close to the equator around 5°S. As such, the Coriolis acceleration becomes ineffective and the January mean easterly $\langle u_{200} \rangle$ is only 1.8 m s^{-1} at 90°E along the equator. An average of July and January mean u_{200} is 7.5 m s^{-1} (easterly), which is nearly identical to the observed annual mean $\langle u_{200} \rangle$ at 0°, 90°E. This leads to the conclusion that the July mean easterly u_{200}, which is enhanced by strong monsoonal convection near 20°N over Southeast Asia, is the major contributor to the annual mean easterly $\langle u_{200} \rangle$ over the central Indian Ocean. This, in turn, implies that monsoonal convection during northern summer is primarily responsible for the enhancement of the annual mean easterly $\langle u_{200} \rangle$ over the equatorial Indian Ocean. Namely, the forcing of these equatorial easterlies does not exist in the immediate vicinity of the equator, but is located over the Asiatic monsoon domain around 20°N.

The equatorial maritime continent between about 100°E and 160°E is a region where the annual variation in u_{200} appears to be minimal. An inspection of Figs. 3b and 4b reveals the prevalence of u_{200} easterlies over the equatorial maritime continent with a nearly equal intensity in both July and January. The July mean u_{200} easterlies correspond to the Rossby response enhanced by Northern Hemisphere summer monsoon rains (Fig. 3), while the January mean u_{200} easterlies are similarly

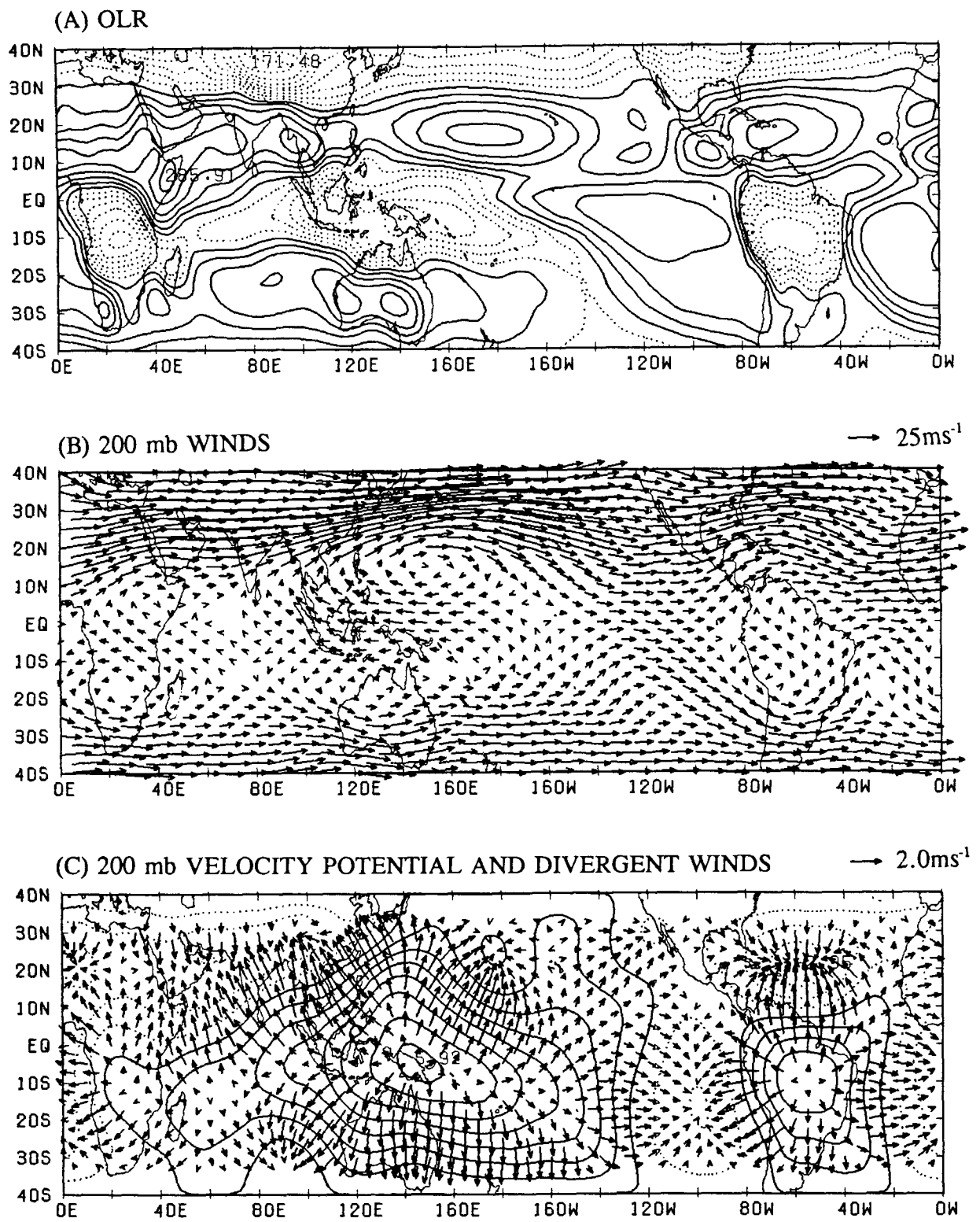

FIG. 4. As in Fig. 2 except for the January mean.

excited by Southern Hemisphere summer monsoon rains (Fig. 4). Hence, the annual mean $\langle u_{200} \rangle$ easterlies are a result of an equal contribution from the northern and southern summer monsoon rains. Consequently, these annual mean $\langle u_{200} \rangle$ easterlies over the equatorial maritime continent do not seem to be directly related

to the annual mean $\langle \text{OLR} \rangle$ over the same region. This may be the reason why $\langle u_{200} \rangle$ is not in quadrature with $\langle \text{OLR} \rangle$.

c. *Local Eliassen–Palm (E–P) fluxes due to annual cycles*

Trenberth (1986) investigated the impact of transient eddies on the time-mean flow using localized E–P flux diagnostics. The primary objective in this subsection is to diagnose the forcing of the annual mean east–west circulation by annual cycles. Any meteorological variable, for example, u, is partitioned into three parts as

$$u = \langle u \rangle + u^* + u', \tag{1}$$

where $\langle u \rangle$ denotes the normal annual mean, u^* normal annual cycles determined from many years of data, and u' transient eddies other than annual cycles. There is no correlation between u^* and u', and thus $\langle u^* u' \rangle = 0$. With the aid of Eq. (A11) of Trenberth, the annual mean $\langle u \rangle$ momentum equation can be expressed by

$$D\langle u \rangle - f\langle v \rangle'' = \frac{1}{\cos\varphi} \nabla \cdot \mathbf{E}_u^* + \langle T_u \rangle + \langle F_x \rangle, \tag{2}$$

where

$$\langle v \rangle'' = \langle v_d \rangle - \frac{1}{\rho_0} \frac{\partial}{\partial z} \frac{\rho_0}{S} \left\langle v^* \frac{\partial \Phi^*}{\partial z} \right\rangle, \tag{3}$$

$$\mathbf{E}_u^* = \left[\frac{1}{2} (\langle v^{*2} - u^{*2} \rangle), -\langle u^* v^* \rangle, \frac{f}{S} \left\langle v^* \frac{\partial \Phi^*}{\partial z} \right\rangle \right], \tag{4}$$

$$\langle T_u \rangle = \frac{1}{\cos\varphi} \nabla \cdot \mathbf{E}_u' + \frac{f}{\rho_0} \frac{\partial}{\partial z} \frac{\rho_0}{S} \left\langle v' \frac{\partial \Phi'}{\partial z} \right\rangle, \tag{5}$$

$$\mathbf{E}_u' = \left[\frac{1}{2} (\langle v'^2 - u'^2 \rangle), -\langle u' v' \rangle, \frac{f}{S} \left\langle v' \frac{\partial \Phi'}{\partial z} \right\rangle \right], \tag{6}$$

$$D = \langle u \rangle \frac{\partial}{\partial x} + \langle v \rangle \frac{\partial}{\partial y} + \langle w \rangle \frac{\partial}{\partial z}, \tag{7}$$

$$\nabla = \left[\frac{\partial}{\partial x}, \frac{1}{\cos\varphi} \frac{\partial}{\partial y} \cos\varphi, \frac{1}{\rho_0} \frac{\partial}{\partial z} \rho_0 \right], \tag{8}$$

$$dx = a \cos\varphi \partial\lambda, \quad dy = a d\varphi, \quad z = \ln(p_0/p), \tag{9}$$

in which Φ denotes geopotential height and S the time-mean static stability; other symbols are the same as those defined by Trenberth. For brevity, several small terms related either to spherical geometry or to the divergence of geostrophic winds arising from the variable f are omitted. As defined in (3), the residual meridional circulation, that is, $\langle v \rangle''$, contains not only annual mean divergent meridional wind $\langle v_d \rangle$, but also meridional circulations induced by vertical differential heat transports due to annual cycles, which change the thermal wind and affect the time-mean momentum balance. Here $\mathbf{E}_u^*$ represents a localized E–P flux vector, while its divergence indicates the impact of annual cycle on the annual mean zonal flow. Similarly, $\mathbf{E}_u'$ represents a localized E–P flux vector due to transient eddies. The second term on the right-hand side of (5) is for the residual meridional circulation induced by heat transports by transient eddies. Unfortunately, the data limitation in the present study inhibits an accurate calculation of $\langle T_u \rangle$.

In order to explore, in a preliminary way, whether localized E–P fluxes due to annual cycles may have played a role on the maintenance of the equatorial annual mean east–west circulation at 200 mb, we first estimate the magnitude of the mean advection term $D\langle u \rangle$, the residual circulation term, $f\langle v \rangle''$, and $\nabla \cdot \mathbf{E}_u^*$ at the same level. From Fig. 1a, the magnitude of $D\langle u \rangle$ is estimated to be about 1×10^{-5} m s^{-2} along the equator. In Fig. 1c, $\langle v_d \rangle$ is on the order of 1 m s^{-1}. Based on the Ramage and Raman (1972) monthly mean temperature and wind data, the magnitude of thermally induced winds near the equator [the second term on the rhs of (3)] is estimated to be about 0.2 m s^{-1} or less. When averaged between 15°N and 15°S (i.e., approximately equal to the Rossby radius of deformation), the magnitude of $f\langle v \rangle''$ is about 1×10^{-5} m s^{-2}.

One of the important characteristics of the Asiatic summer monsoon is a distinct reversal in u and v between summer and winter. This results in weak annual mean $\langle u \rangle$ and $\langle v \rangle$ winds, while monthly mean u^* and v^* anomalies are significant. In July (Fig. 3b), $u^* < 0$ and $v^* < 0$, and hence $u^* v^* > 0$. In fact, the product $u^* v^*$ is positive throughout the year over the Asiatic monsoon domain (i.e., either equatorward transport of easterly momentum or poleward transport of westerly momentum). The annual mean $\langle u^* v^* \rangle$ turns out to be maximum (100 m^2 s^{-2}) near 20°N, 80°W with a substantial flux divergence over the equatorial Indian Ocean. Thus, the y component of the E–P flux divergence becomes negative (easterly acceleration), amounting to about -3×10^{-5} m s^{-2} at 0°, 80°E. Easterly acceleration is further reinforced by the x component of the E–P flux divergence, totaling -3.6×10^{-5} m s^{-2} at the same location. Heat transports due to the Asiatic summer monsoon circulation is equatorward from the heated Asiatic continent (including Tibet) to the cool Indian Ocean, reaching a maximum near 200 mb where the north–south temperature difference is most pronounced. The annual mean heat flux due to annual cycles is also equatorward with a maximum in the upper troposphere. Thus, the z component of the local E–P flux divergence becomes negative (easterly acceleration). However, this baroclinic contribution is relatively small, amounting only to -0.1×10^{-5} m s^{-2}. In summary, the barotropic contribution (i.e., the x and y components of local E–P flux divergence) is primarily responsible for the

maintenance of annual mean $\langle u_{200} \rangle$ easterlies over the equatorial Indian Ocean.

Let us next consider how the annual mean $\langle u_{200} \rangle$ westerlies are maintained over the equatorial eastern Pacific. As can be expected from Figs. 3b and 4b, this is a region of significant flux convergence of westerly momentum due to annual cycles. The y component of $\nabla \mathbf{E}_u^*$, when averaged between 10°N and 10°S along 140°W, turns out to be about 5×10^{-5} m s^{-2} (westerly acceleration). East of 120°W along the equator, the x component also contributes to westerly acceleration of about 2×10^{-5} m s^{-2}. The z component of $\nabla \cdot \mathbf{E}_u^*$, that is, baroclinic contribution is universally small near the equator.

In this subsection, the importance of localized E–P flux vectors upon the maintenance of the annual mean east–west zonal circulation along the equator is confirmed. This, in turn, indicates the importance of annual cycles occurring away from the equator. In near-equatorial latitudes, the E–P flux divergence due to annual cycles appears to be the leading term in (2). Gill's (1980) linear diagnostic model includes neither the nonlinear part of $D\langle u \rangle$, nor the E–P flux divergence in (2). As such, his model does not well simulate the observed annual mean zonal winds along the equator, as already mentioned in section 3.

5. Annual cycle of the equatorial east–west circulation

a. Annual cycle of SST

The SST annual cycle is of fundamental importance for better understanding the annual cycle of the equatorial east–west circulation. A longitude–month section of the annual cycle in SST at the equator is shown in Fig. 5a. The largest amplitude is found off the west coast of South America with a maximum of 1.8°C near 100°W. The highest SST relative to the annual mean appears first in March and April and progressively later in the year as one moves westward toward the central Pacific. At 160°W, SST becomes highest in July. The westward propagation of SST anomalies in the eastern equatorial Pacific has been noted by Bjerknes (1961), Horel (1982), and others. An average westward phase speed is about 24° longitude per month (or 1.0 m s^{-1}). Horel (1982) postulated that the westward propagation of the first SST harmonic is caused by a feedback mechanism between the surface winds and sea surface temperature. The atmospheric response tends to suppress upwelling to the west of the positive SST anomalies and, hence, contributes to the westward propagation of high SST. Meehl (1990) also confirmed the westward propagation in a coarse-grid coupled ocean–atmosphere general circulation model. He lends support to the mechanisms proposed by Horel. Over the Indian Ocean, there exists a distinctly different equatorial regime of the SST annual cycle. Within this regime the SST first harmonic tends to propagate eastward (Fig. 5a). In comparison, the Indonesian seas between about 120° and 160°E are characterized by the minimum amplitude of the first SST harmonic.

The amplitude of the semiannual harmonic in SST along the equator is largest at the western end of the Indian Ocean (Fig. 5b). In this neighborhood, the semiannual harmonic is more important than the annual harmonic. Accordingly, the sum of the first and second SST harmonics (Fig. 5c) also exhibits prominent semiannual character with warm anomalies twice a year in April and November, and cold anomalies in January and August. The Indonesian seas with many large islands scattered between about 100° and 150°E along the equator are also dominated by the semiannual harmonic. Here, SST exceeds the annual mean twice a year (first in late spring and later in late autumn). Below annual mean SST occurs in late winter and late summer. Most probably, the nature of SST annual variation over the Indonesian seas can be explained in terms of the semiannual cycle in solar heating at the equator.

No large island is present along the equator eastward of about 160°E. In this oceanic zone, the amplitude of the SST second harmonic is quite small, being only on the order of 0.1° to 0.2°C (Fig. 5b). Thus, it appears that the ocean response to the semiannual cycle in solar heating is quite small. When the west coast of South America is approached along the equator, the amplitude of the SST first harmonic becomes extraordinarily large (Fig. 5a). In the immediate vicinity of the west coast of South America, the southeasterly trades originated in the Southern Hemisphere subtropics cause substantial annual variations in upwelling.

Figure 5a shows that the east–west SST gradient (relative to the annual mean) between the central (180°) and eastern (100°W) Pacific alternates from a maximum (positive) in March to a minimum (negative) in September, with an approximate amplitude of 0.2°C per 1000 km. The corresponding amplitude of the annual cycle in the north–south SST gradient (anomaly), as estimated between 20°S and 20°N along 160°W and 100°W, is 0.9°C per 1000 km (not shown), which is more than four times as large as that for the east–west SST gradient along the equator. This may be the major reason why the annual variation in the surface meridional wind (low-level Hadley circulation) is much more pronounced than the annual evolution in the surface zonal wind (low-level E–W circulation) along the equator.

b. Annual cycle of surface zonal wind

In Fig. 6a, the u_s first harmonic propagates eastward across the Indian Ocean from 40°E to about 90°E. Conversely, it is of westward-propagating character over the central and eastern Pacific east of 160°E. Recall that the SST first harmonics are also eastward (westward) propagating over the Indian Ocean (central and eastern Pacific). A careful comparison between Figs. 5a and 6a, however, indicates the presence of four

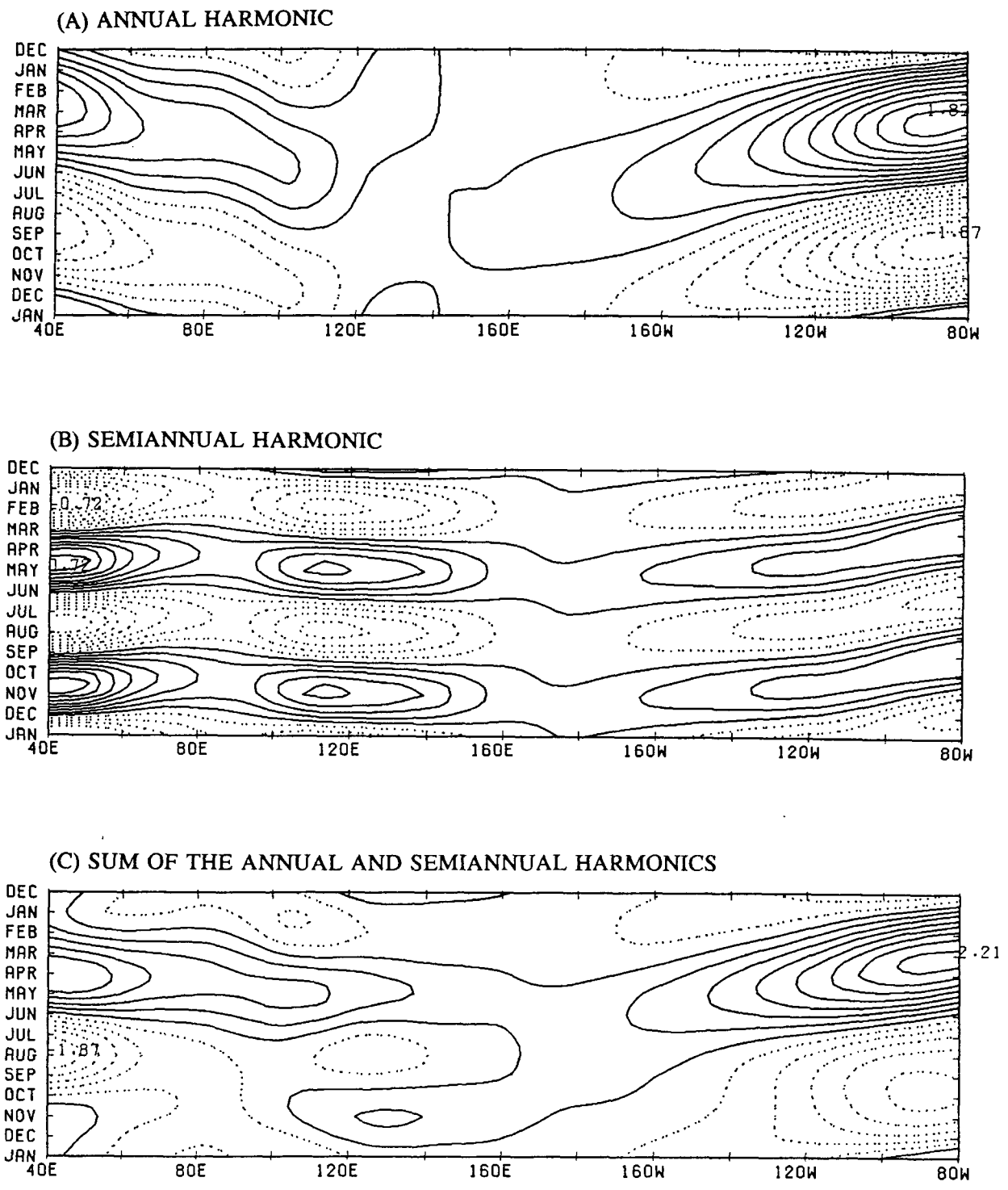

FIG. 5. Month–longitude sections of SST along the equator averaged between 5°N and 5°S: (a) first harmonic (interval 0.2°C), (b) second harmonic (interval 0.1°C), and (c) consolidated (first + second) annual cycle (interval 0.2°C). Dashed lines are for negative SST anomalies.

limited areas of distinctly different phase relation between u_s and SST: namely, (a) Indian Ocean (40°E–80°E), where both SST and u_s first harmonic propagate eastward with the former leading the latter by about three to four months, (b) central Pacific (160°E–140°W) of westward-propagating SST leading u_s first harmonic by about two to four months, (c) eastern Pacific (130°W–100°W), where westward-propagating

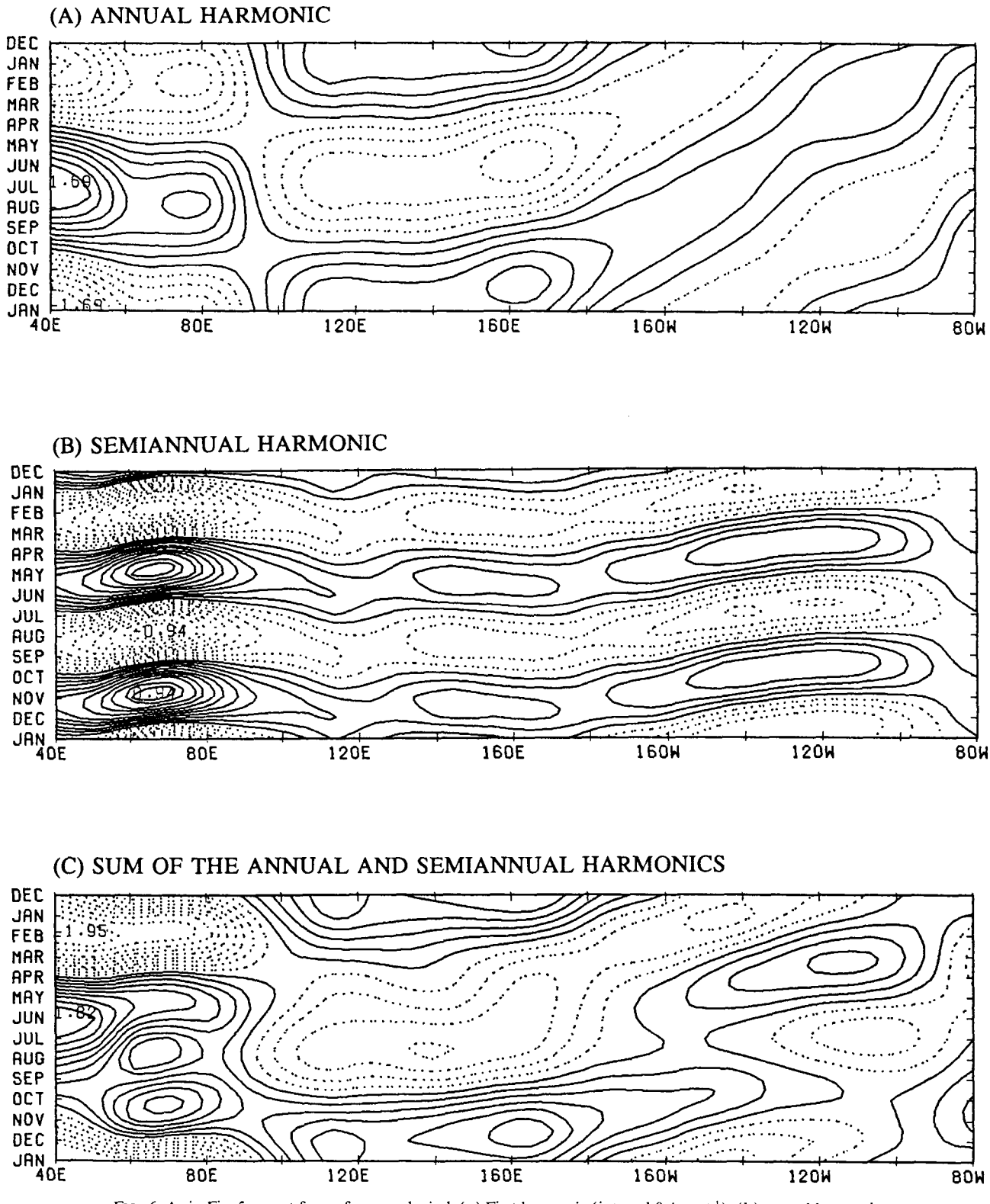

FIG. 6. As in Fig. 5 except for surface zonal wind. (a) First harmonic (interval 0.4 m s^{-1}), (b) second harmonic (interval 0.3 m s^{-1}), and (c) consolidated (first + second) annual cycle (interval 0.4 m s^{-1}).

SST first harmonic lags behind similar signals of westward-moving u_s first harmonic by about one to two months, and (d) South American off shore (90°W–80°W), where u_s first harmonic is inversely correlated with SST first harmonic. Thus, region (c) is the only area where the boundary-layer mechanisms proposed by Horel (1982) are properly working. This is a matter of course because Horel utilized boundary-layer data over the eastern Pacific. At present, why the planetary boundary-layer properties differ significantly with different tropical region is not yet known. It is particularly intriguing to find in region (d) (90°W–80°W) that easterly (westerly) u_s first harmonic is coincident with warm (cold) SST first harmonic in March–April (September–October). Further study is needed.

Between 40°E and 160°E along the equator, the u_s second harmonic (Fig. 6b) is of standing wave character and approximately in phase with the SST second harmonic (Fig. 5b). Namely, westerly u_s coincides with warm SST in April–May and October–November, while easterly u_s is associated with cold SST in January–February and July–August. Perhaps this reflects the semiannual oscillation in solar insolation near the equator. However, one would have to explain why the second harmonics in SST and u_s are in phase. This problem remains unanswered. Between about 180° and 100°W, the u_s and SST second harmonics are both propagating westward, but not in phase (the former leading the latter by about 1.5 month). Again, the boundary layer over region (d) (off the South American west coast) behaves quite differently. Here, the SST second harmonic is approximately out of phase with the u_s second harmonic.

c. *Annual cycle of OLR*

In Fig. 7a, one immediately notes a systematic eastward propagation of OLR anomalies across the Indian Ocean with an approximate phase speed of 10° longitude per month. Between 40°E and about 80°E, the OLR first harmonic is approximately out of phase with the u_s first harmonic, while they lead the SST first harmonic by about two to three months. At 80°E, for example, the highest SST in April occurs about three months before the strongest u_s westerlies in July–August and about four months prior to the OLR minimum (strongest convection) in late August. This is indicative of the importance of planetary boundary-layer processes upon determining convection during the course of the eastward-propagating annual cycles over the Indian Ocean.

Over the equatorial Pacific east of about 160°E, the OLR first harmonic propagates eastward while SST and u_s first harmonics are both westward propagating. Therefore, OLR first harmonic (convection) appears to be independent of planetary boundary-layer parameters such as SST and u_s first harmonics. The semiannual harmonics in SST, u_s, and OLR, however, are nearly in phase (with u_s and OLR slightly leading SST), suggesting a coupled westward propagation in the three fields. The sum of the first and second harmonics shows that when the monthly mean anomaly OLR reaches a minimum (-13 W m^{-2}) at 120°W in April (Fig. 7c), which reflects relatively wet weather at this time of the year over the eastern equatorial Pacific, the monthly mean anomaly SST (Fig. 5c) becomes highest and the monthly mean anomaly u_s (Fig. 6c) is westerly. As such, the planetary boundary-layer processes appear to exert a strong measure of control upon convective activity over this particular area (eastern equatorial Pacific) during particular months (March–April). In the eastern equatorial Pacific the coupled SST–zonal wind westward propagation is evident during the boreal spring (Figs. 5c and 6c), while OLR tends to be stationary (Fig. 7c). These are consistent with Horel (1982) and Wang (1992a, Fig. 3). Quite recently, Murakami (1993) showed westward propagation of original monthly mean OLR anomalies across the equatorial eastern-central Pacific. In that region, the annual cycle involves a direct response to external solar forcing and an active air–sea interaction of the ocean–atmosphere–continent system, as pointed out by Wang (1992b). On the other hand, Meehl (1987) noticed that the monthly mean anomalous OLR averaged between 30°N and 30°S exhibits an eastward propagation. This appears to be primarily a reflection of the annual phase propagation of OLR along the ITCZ, as revealed by Fig. 3 of Wang (1992a).

d. *Annual cycle of 200-mb zonal winds*

Let us now turn our attention to the annual cycle of the upper-level E–W circulation along the equator. Figure 8a reveals that the u_{200} annual harmonic is largely of standing wave character, that is, practically no zonal phase propagation. This stands in sharp contrast with a systematic eastward phase propagation of OLR annual harmonic in Fig. 7a. The amplitude of the u_{200} first harmonic is largest at 70°E, changing from $+6.5$ m s^{-1} (anomaly) in February to -6.5 m s^{-1} (relative to the annual mean) in July. Due to the interference between the first and second u_{200} harmonics, the consolidated u_{200} harmonics in January decrease to 3 to 4 m s^{-1} westerly (see Fig. 8c). Conversely, due to the superposition of the two harmonics, the consolidated u_{200} in July intensifies to -9.5 m s^{-1} (easterly). Thus, over the central Indian Ocean (70°E, 0°), the summer easterly u_{200} becomes much more dominant than the winter westerly u_{200}, that is, summer–winter asymmetry. An inspection of Figs. 6a and 8a reveals an approximate inverse relationship between u_s first harmonics and u_{200} first harmonics over the western Indian Ocean, implying that they are of baroclinic structure in the vertical.

In Fig. 8a, one of the important features over the equatorial eastern Pacific is the dominance of the u_{200}

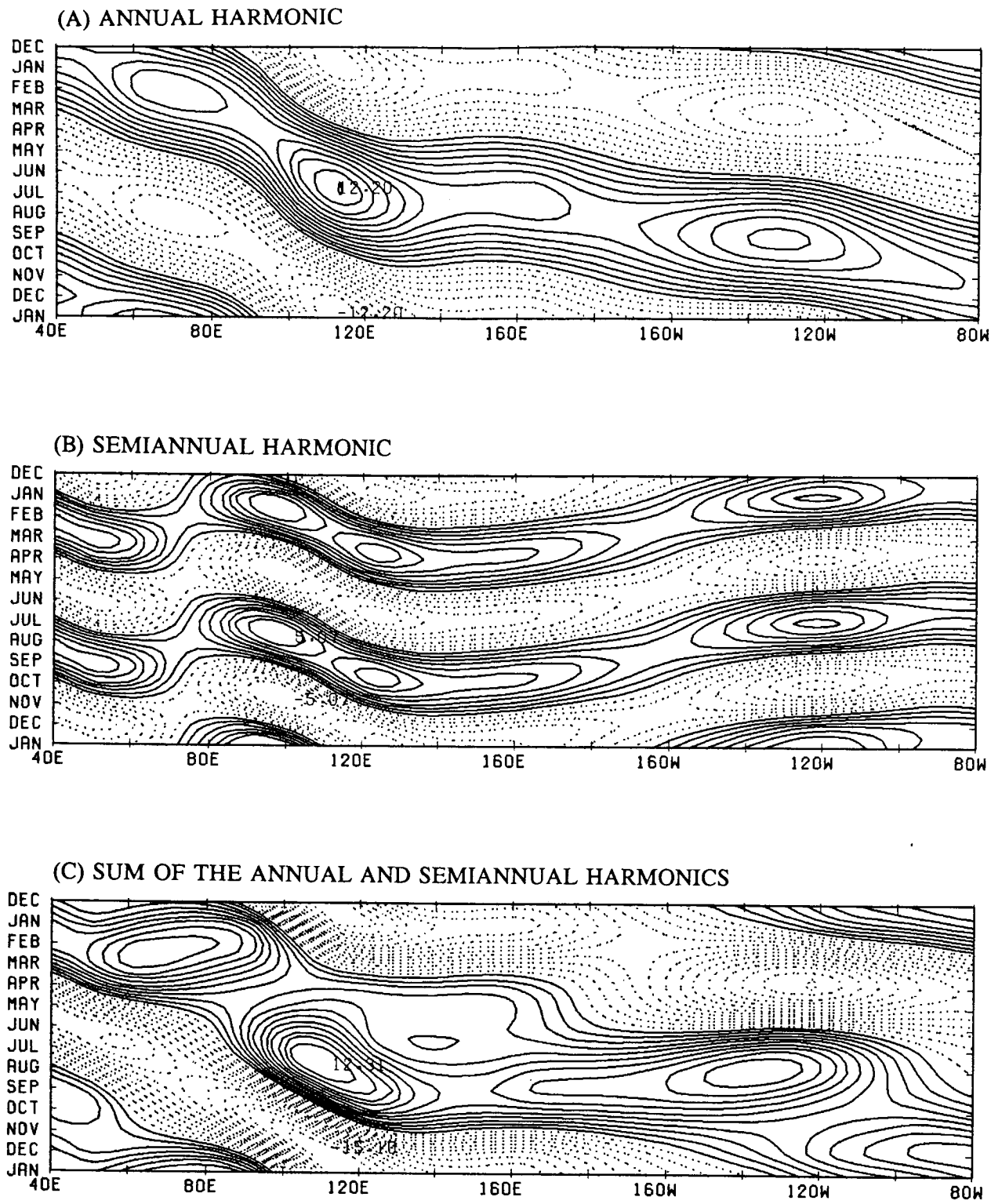

FIG. 7. As in Fig. 5 except for OLR. (a) First harmonic (interval 1.0 W m^{-2}), (b) second harmonic (interval 0.6 W m^{-2}), and (c) consolidated (first + second) annual cycle (interval 1 W m^{-2}).

first harmonic. Since the u_{200} first harmonic is of standing wave character and the OLR first harmonic is of propagating wave character, no apparent relationship exists between these two quantities. Hence, the equatorial OLR first harmonic (annual rainfall variation) is not the major factor in controlling annual changes

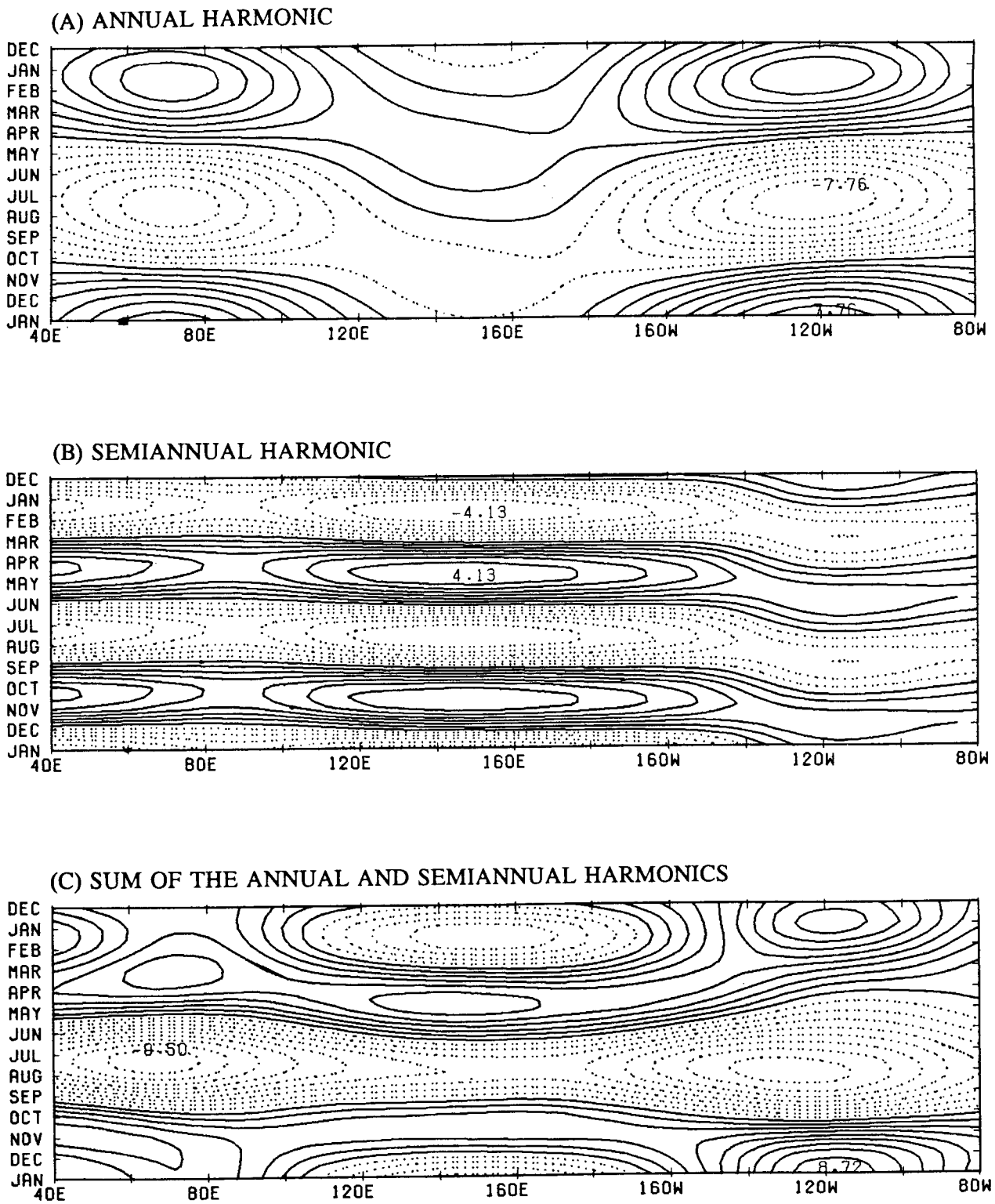

FIG. 8. As in Fig. 5 except for 200-mb zonal wind. (a) First harmonic (interval 1.0 m s^{-1}), (b) second harmonic (interval 0.6 m s^{-1}), and (c) consolidated (first + second) annual cycle (interval 1.0 m s^{-1}).

in the equatorial u_{200} first harmonic. The major controlling factor is the annual cycle in u_{200} dominating in the midlatitude North Pacific. The amplitude of the u_{200} annual cycle exceeds 20 m s^{-1} at 30°N, 120°W (Figs. 3 and 4), while the corresponding amplitude at the equator along the same longitude amounts to only

8 m s^{-1} (Fig. 8c). Furthermore, there exists no systematic correlation between the u_{200} and u_s first harmonics over the equatorial eastern Pacific. This means that the standing u_{200} first harmonic is independent of the westward-propagating u_s first harmonic, which is a key indicator for the planetary boundary-layer processes.

An inspection of Fig. 8c reveals that the sum of the first and second u_{200} harmonic becomes smallest at the beginning of October, that is, just after the autumn equinox. The monthly mean equatorial u_{200} in October is almost identical to the annual mean $\langle u_{200} \rangle$ as shown in Fig. 1a. In fact, not only near the equator but also over the entire global tropics between 40°S and 40°N, the October mean 200-mb wind fields are quite similar to those shown in Fig. 2b for the annual mean 200-mb winds, which are approximately symmetric with respect to the equator. It is then possible that the October mean u_{200} along the equator is under extratropical control, as is the annual mean equatorial $\langle u_{200} \rangle$ (refer to section 3). On the other hand, there is no direct cause-and-effect relationship between OLR* (convection) and u^*_{200} along the equator. In October, u^*_{200} is quite small everywhere along the equator (Fig. 8c) in spite of active convection (negative OLR*) near 90°E (Fig. 7c). A similar argument applies to April (spring equinox). Namely, the April mean 200-mb wind field resembles the annual mean pattern shown in Fig. 2b.

6. Concluding remarks

This study utilized 80 years of sea surface temperatures (SST), surface pressures (p_s), and surface winds (u_s, v_s). Also used are 10 years of data for outgoing longwave radiation (OLR), and 8 years of data for 200-mb winds (u_{200}, v_{200}). For each of the variables, monthly mean data in individual years were averaged by calendar month to obtain normal monthly means for the 12 calendar months. An average of 12 normal monthly mean values corresponds to a normal annual mean, which is signified by a bracket $\langle\ \rangle$. The annual cycle of a variable refers to the month-to-month change in its 12 monthly mean anomaly (relative to the annual mean) and is denoted by an asterisk. The annual cycle is also approximated by the sum of the first and second harmonics.

Some of the characteristic features of annual mean perturbations are detailed in section 3. The annual mean $\langle$OLR$\rangle$ field is nearly symmetric about the equator with active convection over three continents, that is, equatorial Africa, the maritime continent, and equatorial South America. The effect of continentality appears to be more important than the SST effect in enhancing annual mean convection. An approximate in-phase relationship exists between $\langle$OLR$\rangle$ and $\langle u_{200} \rangle$ along the equator. This can be exemplified as follows: $\langle u_{200} \rangle$ is easterly (negative) and minimum directly above the most active convective center (minimum $\langle$OLR$\rangle$) over the maritime continent, while it is westerly (positive) and maximum in regions of maximum $\langle$OLR$\rangle$ (dry weather) over the equatorial eastern Pacific. This is quite different from what is anticipated by Gill's (1980) model of the atmospheric response to a prescribed equatorial heat source. His model displays a u_{200} anomaly in quadrature with the heat source. More specifically, model-produced upper-level winds are easterly (westerly) to the west (east) of the prescribed heating. This then leads us to conclude that the observed annual mean $\langle u_{200} \rangle$ winds along the equator are not really of equatorial convective origin. In section 4, evidence has been presented that they are largely of midlatitude origin. As an example, the origin of $\langle u_{200} \rangle$ westerlies over the eastern equatorial Pacific can be explained as follows. During northern winter, the eastern Pacific is dominated by a distinct westerly duct stretching all the way from about 40°N to 40°S, with prominent equatorial westerlies near 130°W. As the season advances to northern summer, u_{200} becomes slightly easterly near the equator. When averaged throughout the year, however, the annual mean $\langle u_{200} \rangle$ remains westerly and substantial. Thus, the annual cycle occurring in the midlatitude sector of the Pacific plays an important role for the maintenance of annual mean $\langle u_{200} \rangle$ equatorial westerlies near 130°W. This point was further confirmed by examining three-dimensional convergence of localized Eliassen–Palm fluxes. Annual cycles over the extratropical North Pacific are barotropically acting to accelerate the annual mean u_{200} westerlies over the equatorial eastern Pacific. On the other hand, annual cycles over the Asiatic monsoon domain act as a barotropic transient eddy forcing of the annual mean u_{200} easterlies over the equatorial Indian Ocean. In comparison, the baroclinic component, acting through the meridional heat fluxes, appears to contribute little to the maintenance of the annual mean equatorial u_{200} winds over the Indian and Pacific oceans.

In section 5 the annual cycle of an equatorial E–W circulation is described in terms of month–longitude sections of the first and second harmonics of SST, u_s, OLR, and u_{200}. The character of annual cycles is distinctly different between the Indian Ocean and the eastern Pacific. Over the equatorial Indian Ocean, the first harmonics of SST, u_s, and OLR are all propagating eastward, but with different phase speed, that is, u_s moves twice as fast as SST and OLR. There is also a tendency for u_{200} to propagate eastward with an approximate out-of-phase relationship with u_s. Thus, the annually varying E–W circulation over the equatorial Indian Ocean is of baroclinic vertical structure. For example, at 80°E (100°E) along the equator, strongest u_s westerlies are capped by most intense u_{200} easterlies in August (September). However, the timing of highest SST and minimum OLR (most active convection) differs significantly from one longitude to another due to the difference in phase speed between the two variables. At 80°E (100°E), the SST first harmonic reaches its highest value in April (June), while convection be-

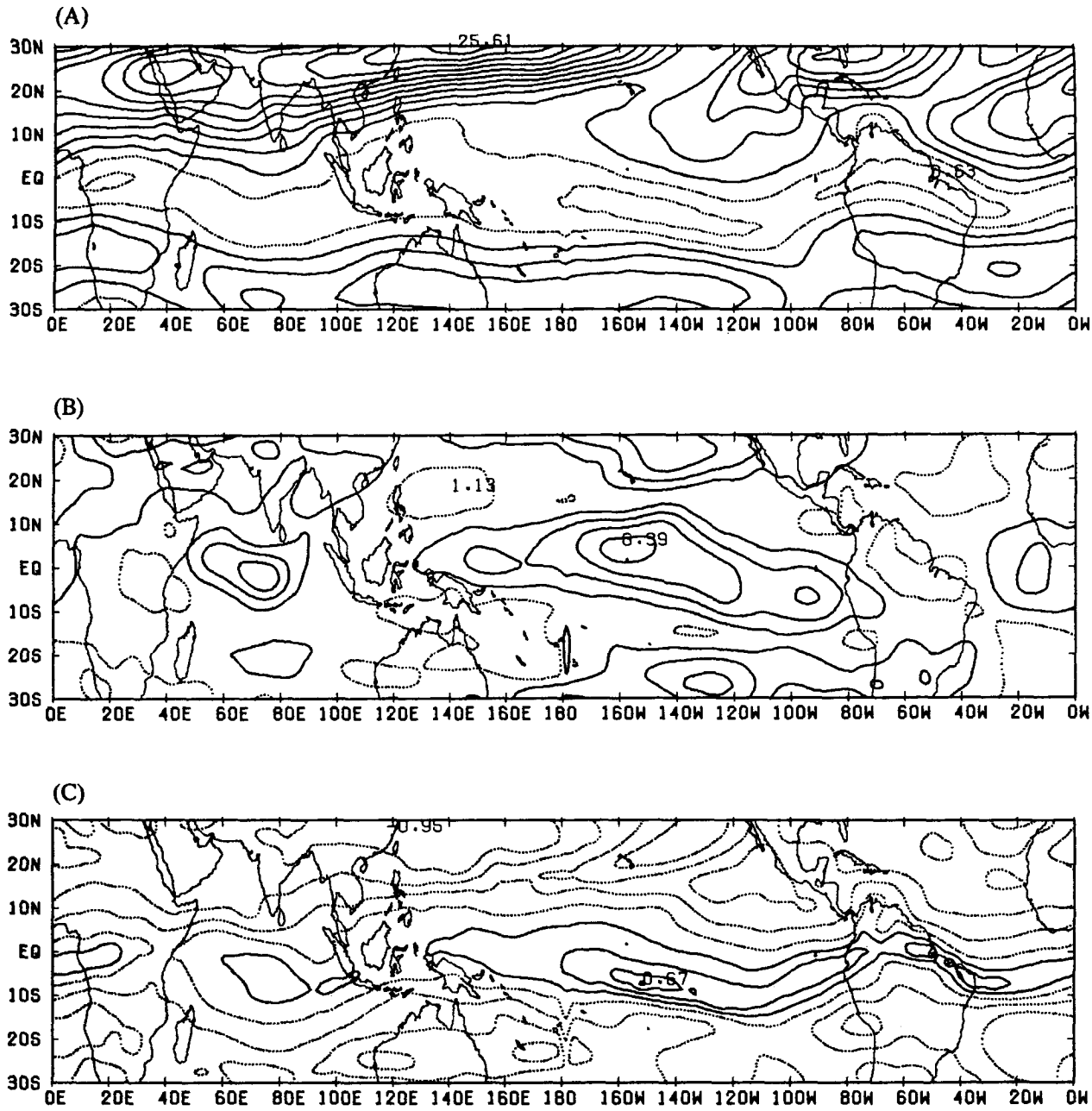

FIG. 9. The standard deviations of the (a) annual cycle, $\sigma(u^*_{200})$ (the contour interval 2 m s^{-1} and the dashed lines less than or equal to 4 m s^{-1}), and (b) interannual component, $\sigma(u_{L,200})$ (the contour interval 1 m s^{-1} and the dashed lines less than or equal to 2 m s^{-1}) of the 200-mb zonal wind. (c) Ratio $\sigma(u_{L,200})/\sigma(u^*_{200})$ in a logarithmic scale (interval 0.2, and dashed lines less than or equal to zero). Refer to the text for further information.

comes most active in September (October). As such, SST is not a primary factor in controlling the annual cycle in convection over the equatorial Indian Ocean.

Similarly, the annually varying E–W circulation over the eastern equatorial Pacific is not sensitive to the annual cycle in convection. Here, OLR is of propagating wave character, while u_{200} is of standing wave character with the largest annual amplitude near 140°W–100°W. The u_{200} annual cycle over the equatorial eastern Pacific is largely controlled by the u_{200} annual variations occurring in the extratropics of each hemisphere. Furthermore, u_{200} appears to be nearly independent of the planetary boundary-layer processes, since both SST and u_s propagate westward as opposed to standing u_{200} perturbations. In the boreal spring, SST becomes highest in association with strongest u_s westerlies. This lends

support to the boundary-layer mechanisms proposed by Horel (1982) for westward-propagating surface signals across the equatorial eastern Pacific.

The nature of annual cycles, as summarized above, appears to be quite different from the character of interannual variations. Many authors (e.g., Arkin and Webster 1985; Wang and Murakami 1988; Webster and Yang 1989, 1992; Wang 1992c) have pointed out that convection plays a key role for the determination of location and intensity of interannual variations in the equatorial E–W circulation. The different character between the annual cycles and interannual variations can be more firmly confirmed by evaluating the standard deviations of u^*_{200} (annual cycle in u_{200}) and $u_{L,200}$ (interannual variations in u_{200}). In Figs. 9a and 9b, the former standard deviation is predominant in the southern and northern extratropics, while the latter is prominent in the equatorial latitudes. Hence, the interannual variation in $u_{L,200}$ is of equatorially trapped character. Along the equator, $\sigma(u_{L,200})$ exhibits three maxima in excess of 4 m s^{-1} at the central Indian Ocean (50°–80°E), the central and eastern Pacific (170°E–100°W), and the central Atlantic Ocean (20°–10°W), respectively. Note that these equatorial oceanic regions of large $\sigma(u_{L,200})$ are nearly identical to those with substantial $\sigma(u^*_{200})$. Presumably, this is indicative of a spatial phase lock between the $u_{L,200}$ interannual variation and u^*_{200} annual variation along the equator.

Across the North and South Pacific between about 160°W and 110°W is a meridional-oriented train of large $\sigma(u_{L,200})$ with maxima near 25°–30°N, 5°N–5°S, and 25°–30°S, respectively. A similar meridional train of large $\sigma(u_{L,200})$, although less distinct, also exists over the India–Indian Ocean region between about 60°E and 90°E. These features are perhaps indicative of an important role of lateral coupling in the excitement of interannual variations in u_{200}. This lateral coupling and its phase locking with the seasonal cycle require further investigation. Figure 9c depicts the ratio between $\sigma(u_{L,200})$ and $\sigma(u^*_{200})$ in a logarithmic scale and indicates the dominance of interannual variations as compared with annual variations over a large part of the equatorial zone between 5°N and 10°S. Away from the equatorial zone, the latter dominates the former. As such, the interannual variability of $u_{L,200}$ appears to be forced by different mechanisms than the annual variability of u^*_{200}. Unfortunately, why the physical processes are a function of climate epoch is not yet known.

Acknowledgments. The authors are indebted to Dr. P. J. Webster for his invaluable and constructive comments on the momentum and heat balance of the annual mean equatorial zonal winds; as a result, the exposition has been much improved. The authors also thank Dr. T. A. Schroeder and anonymous reviewer's comments on the original version of the manuscripts. Thanks are also due to Ms. Joanne Houng for her assistance in data processing and Ms. Twyla Thomas for editing of this manuscript. This research is supported by the EPOCS program of NOAA under Grant NA-90-RAH00074.

REFERENCES

Arkin, P., and P. J. Webster, 1985: Annual and interannual variability of tropical–extratropical interactions: An empirical study. *Mon. Wea. Rev.*, **113,** 1510–1523.

Bjerknes, J., 1961: El Niño study based on analysis of ocean surface temperature. *Inter-Amer. Trop. Tuna Comm. Bull.*, **5,** 219–221.

——, 1969: Atmospheric teleconnection from the equatorial Pacific. *Mon. Wea. Rev.*, **97,** 163–172.

Dorman, C. E., and R. H. Bourke, 1979: Precipitation over the Pacific Ocean, 30°S to 60°N. *Mon. Wea. Rev.*, **107,** 896–910.

Gill, A. E., 1980: Some simple solutions for heat-induced tropical circulation. *Quart. J. Roy. Meteor. Soc.*, **106,** 447–462.

Hastenrath, S., and P. Lamb, 1978: *Climatic Atlas of the Tropical Atlantic and Eastern Pacific Oceans.* University of Wisconsin Press, 122 pp.

Horel, J. D., 1982: On the annual cycle of the tropical Pacific atmosphere and ocean. *Mon. Wea. Rev.*, **110,** 1863–1878.

Hsu, C.-P., and J. M. Wallace, 1976: The global distribution of the annual and semiannual cycles in sea-level pressure. *Mon. Wea. Rev.*, **104,** 1093–1103.

Krishnamurti, T. N., 1971: Tropical east–west circulation during the northern summer. *J. Atmos. Sci.*, **28,** 1342–1347.

Lau, K. M., and H. Lim, 1984: On the dynamics of equatorial forcing of climate teleconnections. *J. Atmos. Sci.*, **41,** 161–171.

Lim, H., and C.-P. Chang, 1983: Dynamics of teleconnections and Walker circulations forced by equatorial heating. *J. Atmos. Sci.*, **40,** 1897–1915.

Meehl, G. A., 1987: The annual cycle and interannual variability in the tropical Pacific and Indian Ocean regions. *Mon. Wea. Rev.*, **115,** 27–50.

——, 1990: Seasonal cycle forcing of El Niño Southern Oscillation in a global, coupled ocean–atmosphere model. *J. Climate,* **3,** 72–98.

Mitchell, T. P., 1990: The annual march of convection, sea surface temperature, and surface winds in the tropics. Ph.D. thesis. University of Washington, 175 pp.

Motell, C. E., and B. C. Weare, 1987: Estimating tropical Pacific rainfall using digital satellite data. *J. Climate Appl. Meteor.*, **41,** 604–613.

Murakami, T., 1974a: Steady and transient waves excited by diabatic heat sources during the summer monsoon. *J. Atmos. Sci.*, **31,** 340–357.

——, 1974b: Atmospheric response to heat sources during July. UHMET-74-04, Department of Meteorology, University of Hawaii, Honolulu, HI.

——, 1978: Regional energetics of the 200 mb summer circulations. *Mon. Wea. Rev.*, **106,** 614–628.

——, 1987: Effects of the Tibetan Plateau. *Monsoon Meteorology,* C.-P. Chang and T. N. Krishnamurti Eds. Oxford University Press, 235–270.

——, 1993: Relationship between monsoon and annual variation of SST over the eastern Pacific. *Tenki, Meteor. Soc. Japan,* in press.

——, and M. S. Unninayar, 1977: Atmospheric circulation during December 1970 through February 1971. *Mon. Wea. Rev.*, **105,** 1024–1038.

——, L.-X. Chen, and A. Xie, 1986: Relationship among seasonal cycles, low-frequency oscillations and transient disturbances as revealed from outgoing longwave radiation data. *Mon. Wea. Rev.*, **114,** 1456–1465.

Philander, S. G., 1990: *El Niño, La Niña, and the Southern Oscillation.* Academic Press, 293 pp.

Ramage, C. S., and A. M. Hori, 1981: Meteorological aspects of El Niño. *Mon. Wea. Rev.*, **109,** 1827–1835.

——, and C. V. R. Raman, 1972: *Meteorological Atlas of the International Indian Ocean Expedition. Volume 2.* U.S. Government Printing Office, Washington D.C., Catalog No. 72-600068.

Rasmusson, E. M., and T. H. Carpenter, 1982: Variations in tropical sea surface temperature and surface wind fields associated with the Southern Oscillation/El Niño. *Mon. Wea. Rev.*, **110**, 354–384.

——, X.-L. Wang, and C. F. Ropelewski, 1990: The biennial component of ENSO variability, *J. Marine Sys.*, **1**, 71–96.

Sadler, J. C., M. A. Lander, A. M. Hori, and L. K. Oda, 1987: *Tropical Marine Climatic Atlas, Vol. 2., Pacific Ocean.* UHMET 87-02, Department of Meteorology, University of Hawaii, Honolulu, HI.

Sardeshmukh, P. D., and I. M. Held, 1984: The vorticity balance in the tropical upper troposphere of a general circulation model. *J. Atmos. Sci.*, **41**, 768–778.

——, and B. J. Hoskins, 1988: On the generation of global rotational flow by steady idealized tropical divergence. *J. Atmos. Sci.*, **45**, 1228–1251.

Taylor, R. C., 1973: An Atlas of Pacific Island Rainfall. Data Rep. No. 25, HIG-73-9, Hawaii Institute of Geophysics, 175 pp. [NTIS AD767073].

Trenberth, K. E., 1986: An assessment of the impact of transient eddies on the zonal flow during a blocking episode using localized Eliassen–Palm flux diagnostics. *J. Atmos. Sci.*, **43**, 2070–2087.

——, and J. G. Olson, 1988: An evaluation and intercomparison of global analysis from the National Meteorological Center and the European Center for Medium-Range Weather Forecasts. *Bull. Amer. Meteor. Soc.*, **69**, 1047–1057.

Wallace, J. M., T. P. Mitchell, and C. Deser, 1989: The influence of sea surface temperature on surface wind in the eastern equatorial Pacific: seasonal and interannual variability. *J. Climate*, **2**, 1492–1499.

Wang, B., 1992a: Climatic regimes of tropical convection and rainfall. *J. Climate*, submitted.

——, 1992b: On the annual cycle in the equatorial Pacific cold tongue. *J. Climate*, submitted.

——, 1992c: The vertical structure and evolution of the ENSO anomaly mode during 1979–89. *J. Atmos. Sci.*, **49**, 698–712.

Wang, X.-L., and T. Murakami, 1988: Intraseasonal disturbance activity before, during and after the 1982–83 ENSO. *J. Atmos. Sci.*, **45**, 3754–3770.

Weare, B. C., P. T. Strub, and M. D. Samuel, 1980: Marine Climate Atlas of the Tropical Pacific Ocean. Dept. Land, Air and Water Resources, University of California, Davis, 147 pp.

Webster, P. J., and J. R. Holton, 1982: Cross-equatorial response to mid-latitude forcing in a zonally varying basic state. *J. Atmos. Sci.*, **39**, 722–733.

——, and S. Yang, 1989: The three-dimensional structure of perturbation kinetic energy and its relationship to the zonal wind. *J. Climate*, **2**, 1186–1198.

——, and ——, 1992: Monsoons and ENSO: Selectively interactive systems. *Quart. J. Roy. Meteor. Soc.*,

Wyrtki, K., and G. Meyers, 1975: The trade wind field over the Pacific Ocean. Part I: The mean field and the mean annual variation. Rep. No. HIG-75-1, Hawaii Institute of Geophysics, 26 pp.

——, and ——, 1976: The trade wind field over the Pacific Ocean, *J. Meteor.*, **15**, 698–704.

Young, J. A., 1987: Physics of monsoons: The current view. *Monsoons.* J. S. Fein and P. L. Stephens Eds. John Wiley and Sons, 211–243.